The 5th International Symposium - Supercritical CO_2 Power Cycles
March 28-31, 2016, San Antonio, Texas

Experimental Assessment of Thermodynamic Properties for Metastable CO_2

Authors

Derek Paxson

Derek Paxson is a master's degree candidate in aerospace engineering at the Massachusetts Institute of Technology Gas Turbine Lab. His research interests include power generation, aircraft propulsion, rocket propulsion, and automotive engine modelling/testing

Claudio Lettieri

Claudio Lettieri is Assistant Professor at the faculty of Aerospace Engineering at Delft University of Technology. His research interests include internal flows in turbo machinery, multiphase flows, non-ideal compressible fluid dynamics and cavitation in turbopumps.

Zoltan Spakovszky

Zoltan Spakovszky is Professor of Aeronautics and Astronautics at the Massachusetts Institute of Technology and the director of the Gas Turbine Laboratory. His principal fields of interest include internal flows in turbomachinery, compressor aerodynamics and stability, dynamic system modeling of aircraft gas turbine engines, micro-scale gas bearing dynamics, and aero-acoustics.

Peter Bryanston-Cross

Peter Bryanston-Cross is an emeritus professor at the University of Warwick, UK where he spent 10 years building up the Optical Engineering Laboratory. He is currently working as a consultant in flow visualization and optical phase measurement. In addition to his consulting work, Peter is also a visiting professor at Changchun University, China.

Akihiro Nakaniwa

Akihiro Nakaniwa is a project manager at The Research & Innovation Center, Technology & Innovation Headquarters, Mitsubishi Heavy Industries, Ltd. He has worked on the aerodynamic design and development of centrifugal compressors for 15 years. Mr. Nakaniwa has an M.S. degree from Kyushu University in Japan.

Abstract

Advanced compressors for supercritical CO_2 (S-CO_2) are a key enabling technology for carbon capture and sequestration (CCS), enhanced oil recovery (EOR), and power cycles. For example in CO_2 compressor applications, the thermodynamic state of the working fluid is close to the two-phase region where phase change effects are important. The expansion near the leading edge of the compressor blades can cause localized condensation, which in turn results in performance and stability issues. The rapid rate of expansion in this region leads to non-equilibrium condensation with the fluid becoming a metastable subcooled vapor. Numerical assessment is essential to guide the design of these compressors, but multi-phase models are difficult to implement due to the lack of suitable metastable phase properties. Single-phase calculations can be used under certain conditions if the equilibrium gas properties can be extrapolated into the metastable vapor region. Through a combined computational and experimental campaign, this paper aims to provide an initial validation of two approaches to determine metastable properties: a spline-based extrapolation of equilibrium properties and equation of state (EOS) based extrapolation using the NIST Reference Fluid Thermodynamic and Transport Properties Database (RefProp) formulation of the Span and Wagner equation of state. The models are verified through a laboratory scale high-pressure blowdown rig, which includes a modular converging-diverging nozzle test section. Density and pressure measurements are obtained using a shearing interferometer and high frequency pressure transducers respectively. The measurements confirm the viability of direct metastable extrapolation, as well as validating shearing interferometry and high-speed pressure measurements as a means to fully characterize the metastable state of supercritical CO_2.

Introduction

Stable and efficient operation close to the two-phase region is desirable for super-high pressure CO_2 compressors used for carbon capture and sequestration (CCS) and enhanced oil recovery (EOR). The key benefits are reduced overall power requirements via lower stage inlet temperatures, and increased power densities through the high densities of CO_2 near the critical point [1]. While the bulk fluid properties generally remain single-phase, flow acceleration near the impeller blade leading edge can result in localized excursions into the two-phase region [1], [2]. Figure 1 illustrates this behavior in a T-s diagram. While two-phase modeling is usually applied to investigate the internal flow behavior in turbomachinery with saturating fluids, a key feature of S-CO_2 compressors allows for the use of single-phase calculations, greatly simplifying the numerical approach. The rapid rate of expansion, and subsequent rapid compression, make the phase change process fundamentally non-equilibrium. A

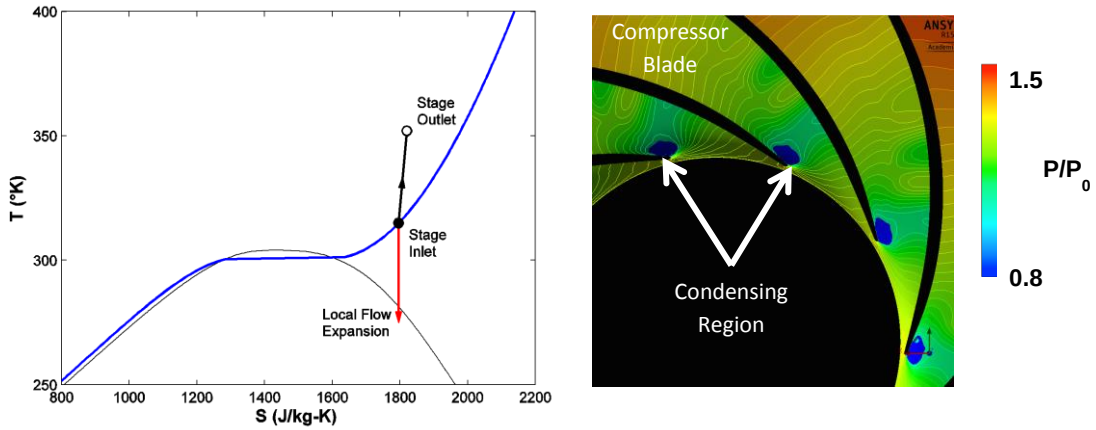

Figure 1: T-s diagram of typical stage operating conditions for a S-CO2 compressors: the nucleation time is much longer than the flow residence time near the impeller leading edge so that condensation is not likely to occur.

previous scaling analysis defined a non-dimensional parameter based on the ratio of through flow time to nucleation time to assess under what conditions condensation would occur. At the leading edge of a typical compressor blade, this ratio is of order 10^{-4}, indicating that the nucleation time is much longer than the residence time of a fluid particle, and that condensation is not likely to occur [2]. Further supporting the hypothesis that single-phase calculations can be successfully used is the small relative size of the regions where condensation could occur. Several studies in the literature, for example [1] and [2], suggest that the extent of the condensation region is of the order of 1% of the blade chord.

During rapid cooling, the fluid enters a metastable state where the fluid continues to behave like a gas until the stability limit, the so called Wilson line or spinodal limit, is reached, or there is sufficient nucleation to initiate bulk condensation [3]. This non-equilibrium process, graphically represented in Figure 2, is difficult to measure and an accurate characterization of the meta-stable thermodynamic properties remains a key challenge.

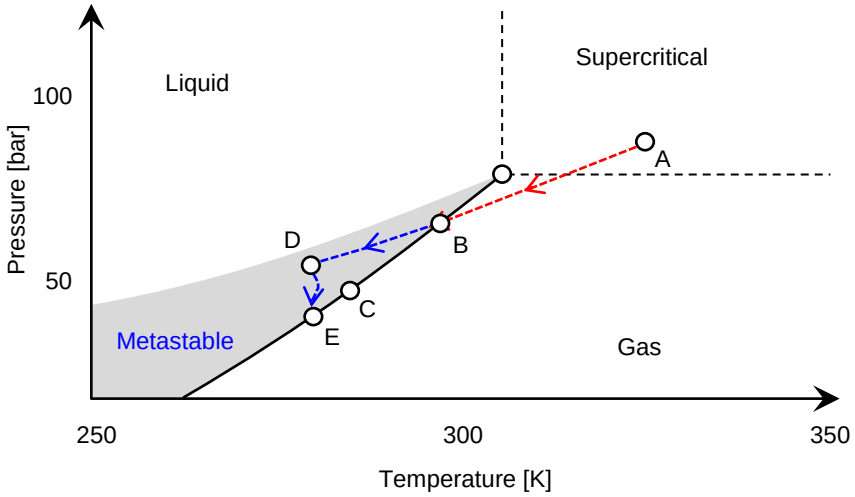

Figure 2: Pressure temperature diagram illustrating the difference between equilibrium and non-equilibrium phase change during an expansion. The short time scales typically encountered in compressors lead to fluid following path A-B-D rather than the equilibrium process A-B-C.

A limited amount of work has been reported in the literature on metastable CO_2, especially near the critical point. Away from the critical point, the equilibrium and metastable vapor can be modelled as an ideal gas. Duff studied non-equilibrium condensation of CO_2 at pressures of one order of magnitude lower than those seen in an S-CO_2 compressor [4]. For an ideal, calorically perfect vapor a general numerical methodology was described to determine thermal choking due to finite rate (non-equilibrium) condensation in high speed flows [5]. However, near the critical point, CO_2 exhibits significant non-ideal behavior and these approaches are not appropriate [6].

Much effort has been put into accurately characterizing the metastable state of water vapor due to its prevalence as a working fluid in the power generation industry. For example in 1997 the International Association for the Properties of Water and Steam (IAPWS) released the most widely used collection of tabulated steam properties. A dense-gas EOS was extrapolated into the metastable vapor region to establish the thermodynamic properties. Despite this, there is still no experimental data with which to compare the extrapolated properties [7]. The state-of-the-art representation of the real-gas properties of CO_2 is the Span and Wagner model. NIST RefProp uses this formulation to calculate equilibrium

properties as well as metastable vapor and liquid properties, but again, these values have no experimental basis. [8].

Cubic spline extrapolation was used in [2] to extend real-gas properties calculated by the Lee-Kessler Model into the metastable region. Experimental pressure measurements demonstrated good agreement away from the critical point; however, the method broke down at the critical point due to inaccuracies in the extrapolation scheme caused by the large gradients of thermodynamic properties.

Scope of the Paper

The objectives of this paper are to experimentally characterize the metastable state and to assess the applicability and the limitations of the cubic spline extrapolation and the direct extrapolation based on the NIST Span and Wagner equation of state model. More specifically the paper addresses the following research questions: (1) can shearing interferometry be used to optically measure the metastable vapor properties at the relevant density and pressure levels of super high-pressure ratio CO_2 compressors, and (2) based on these experimental data, can single-phase real-gas calculations be used to characterize the internal flow behavior in S-CO_2 compressors, and if so, under what conditions.

The technical approach combines numerical computations with experiments. A laboratory-scale experimental blowdown test rig with an instrumented converging-diverging nozzle was used as a surrogate for the flow conditions around the leading edge of a typical S-CO_2 compressor blade. A linear array of high frequency response piezoelectric pressure transducers together with a first-of-its-kind shearing interferometer to measure the density field were used to characterize the internal flow behavior. The paper discusses in detail the methodology and related challenges in the design and construction of the experimental apparatus. Density measurements using the interferometer are compared with results from the extrapolation schemes to assess the validity of these approaches at operating points near the critical point.

Technical Approach

Details of the extrapolation method used to create the metastable properties in the supersaturated vapor region can be found in Refs. [2] [6]. An overview of the extrapolated metastable region is given in Figure 3. The metastable and equilibrium properties calculated from the Span and Wagner EOS were generated with NIST's RefProp version 9.1 [9]. All computational studies were carried out using ANSYS CFX 15 with tabular real-gas properties.

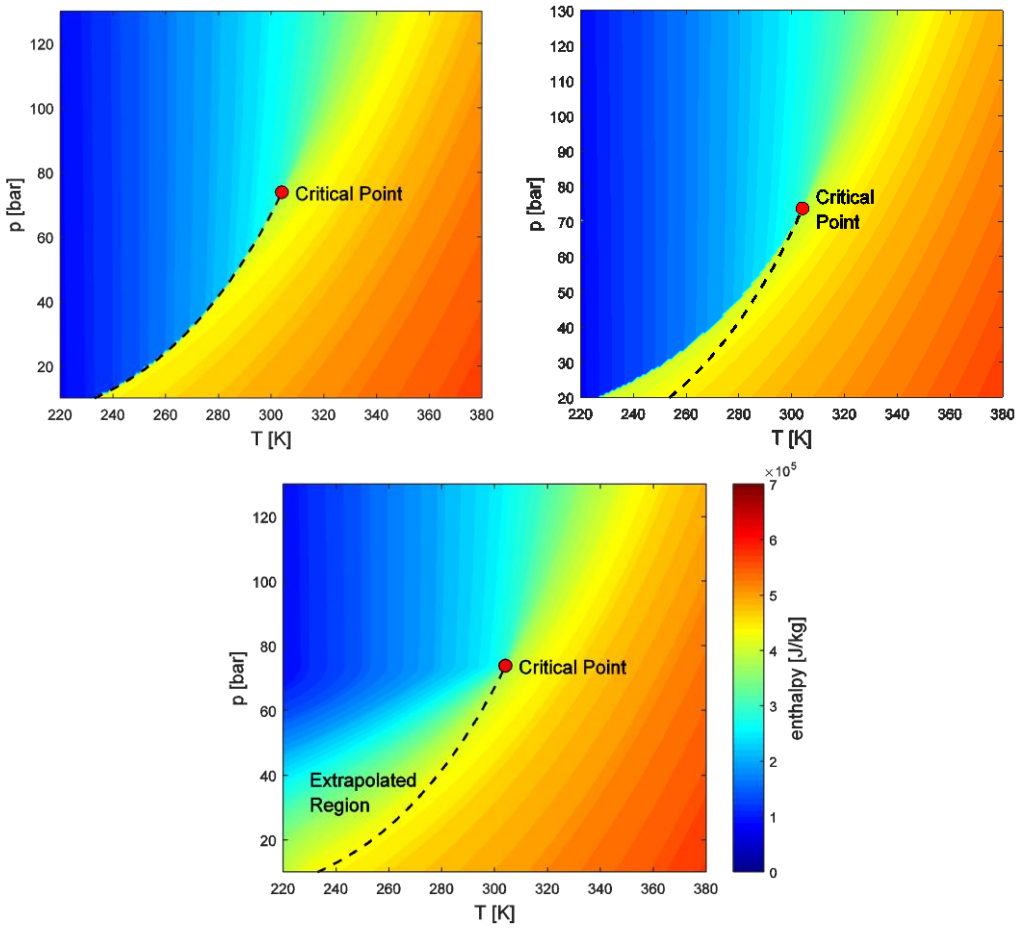

Figure 3: Comparison between equilibrium CO_2 enthalpy values (top left), those extrapolated into the metastable vapor region (bottom), and those calculated through RefProp (top right)

Experimental Blowdown Rig

Several experimental techniques for measuring density in multi-phase flows can be found in the literature. Interferometry was used by Lamanna [10] to measure the density through, and location of, condensation shocks in the diverging section of a converging-diverging nozzle. The working fluid was a mixture of nitrogen and water vapor. While this study was similar to that discussed in the present paper, experiments were carried out with low density nitrogen used as a carrier gas for condensing water droplets which allowed for standard interferometric practices. Also, the operating pressures were

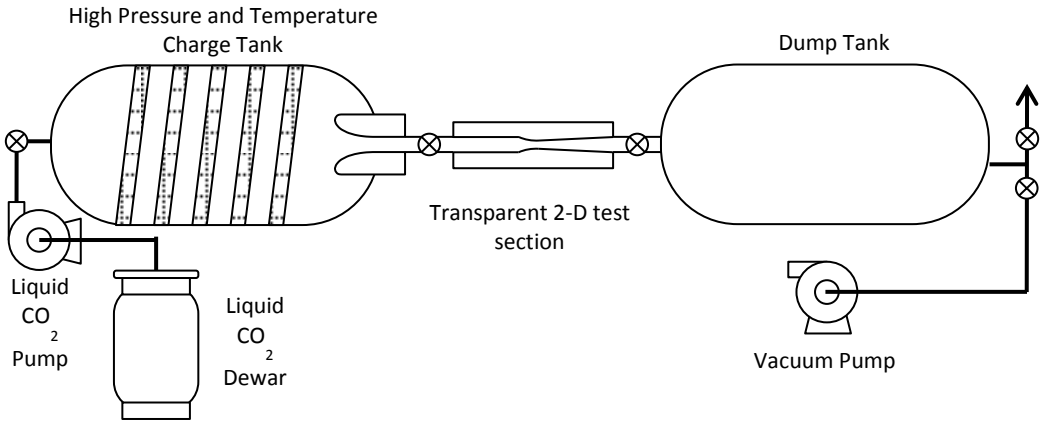

Figure 4: Schematic of the S-CO_2 blowdown rig.

of order 1 bar with much less challenging structural considerations. Density and condensation shock location measurements were conducted by Duff [4] in subcritical CO_2. While the working pressures of order 10 bar were significantly higher than those in [10], the supercritical CO_2 experiments discussed here are at pressures yet one order of magnitude greater than in the literature.

The experimental test apparatus developed in the present paper is based on a high-pressure blowdown test rig with optical access. A schematic of the test rig is shown in Figure 4. CO_2 is pumped from a liquid storage Dewar into a high-pressure heated charge tank, where it is brought to the appropriate stagnation conditions. Fast-acting vales direct the CO_2 through an instrumented test section and into a dump tank. The charge tank allows for stagnation conditions up to 236 bar and 400K. The operating range of the test rig is shown below on a T-s diagram in Figure 6. Due to the high pressure gradients at elevated temperatures in a constant volume tank and the related risk of over-pressurization, the operating limits of the tank were de-rated to 150 bar and 380K.

Test-Section Design

The test section is comprised of a rectangular cross section with a converging-diverging nozzle. Transparent windows on the side faces provide optical access and the top and bottom faces of the nozzle form the nozzle contour and contain taps for static pressure measurements. This arrangement is illustrated in the top image of Figure 5. The functional requirements of the test section are to (1) allow for optical access, (2) facilitate easy and inexpensive changes in nozzle geometry, and (3) provide high downstream pressure measurement resolution in order to detect condensation.

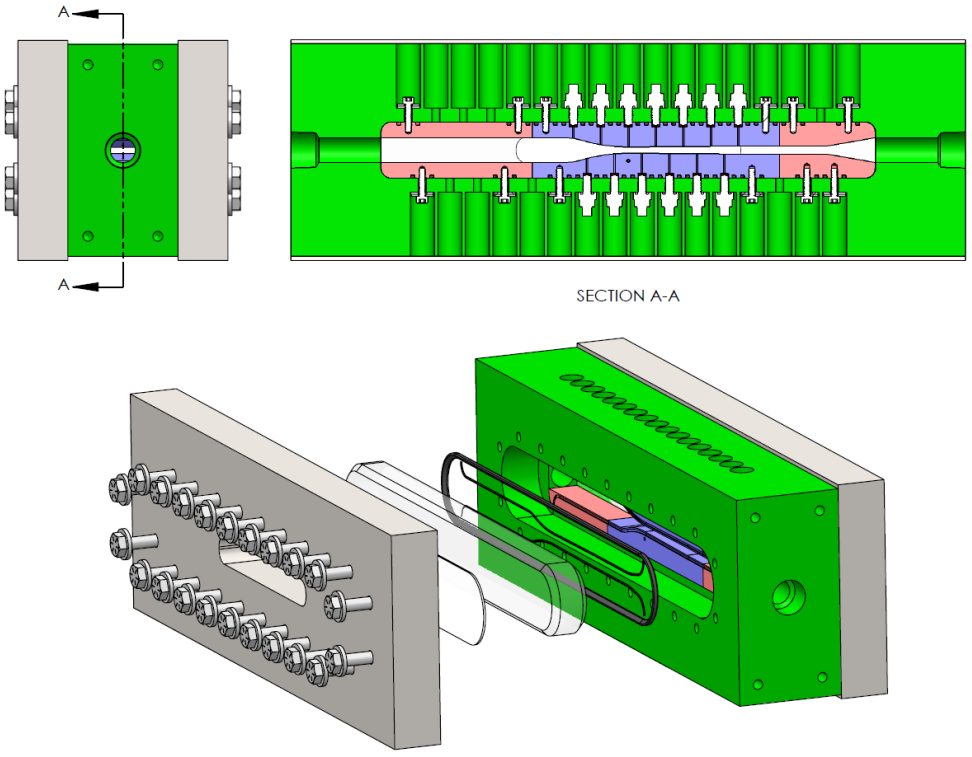

Figure 5: CAD model of test section: Top Image is a centerline cross section showing the purple nozzle inserts and the pressure transducers. Bottom image shows an exploded view of one of the two fused silica windows and sealing features

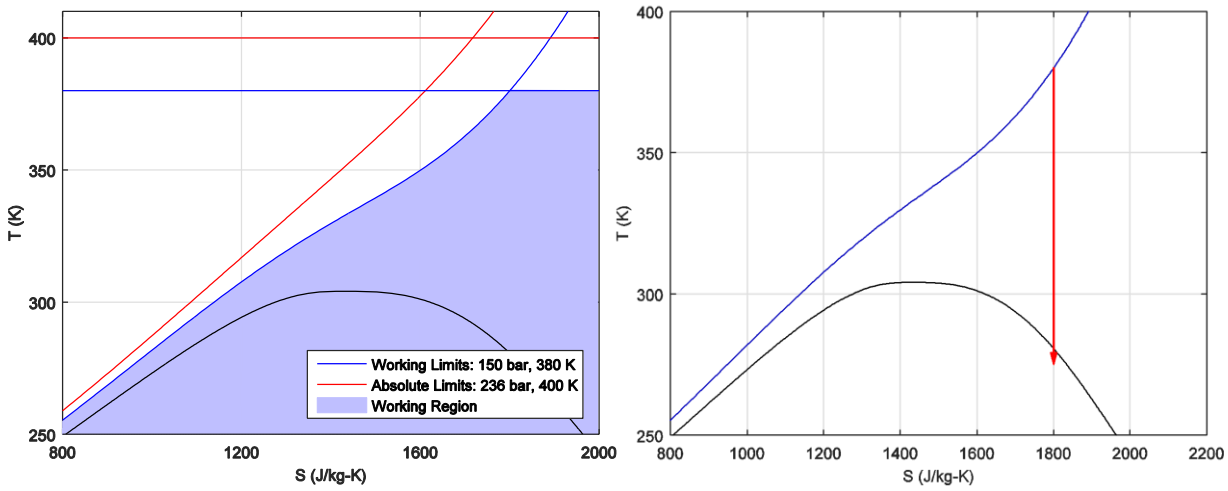

Figure 6: Range of achieved test rig stagnation conditions together with a typical, isentropic blowdown experiments

Optical access was achieved through the use of 19mm fused silica (quartz) windows on either side of the nozzle section. To achieve two-dimensional flow conditions so as to simplify the optical flow analysis, a rectangular cross-section was chosen. Three-dimensional CFD computations of the nozzle geometry confirmed the two-dimensionality of the flow, showing a maximum transverse boundary layer thickness of approximately 3% of the channel width at typical operating conditions. Easy geometry changes were facilitated by divorcing the structural requirements of the test-section from the geometric constraints of the nozzle. A large stainless steel structure (shown in green in Figure 5) retains the windows, and withstands the pressure forces inside the test-section. Inexpensive aluminum inserts (shown in purple) are then bolted into the main body establishing the converging-diverging flow path. The throat height was made as small as possible while still allowing optical access. This was done in order to minimize the mass flow rate and maximize the blowdown time without a significant change in stagnation conditions of the charge tank. The expansion ratio after the throat was determined such that a blowdown from the operating limits of the tank would result in single phase flow through the entire nozzle. This is illustrated in Figure 6.

Shearing Interferometer Design

In addition to pressure measurements, density measurements are required to determine the thermodynamic properties of the CO_2. Interferometry was chosen as the preferred density measurement method as it allows for both qualitative and quantitative analysis. Similar to Schlieren and shadowgraph techniques, interferometry relies on the dependence of refractive index on density in a transparent material [11] [12]. Previous literature confirms that interferometry can be successfully used to measure density in similar geometries with errors below 5% [4], [10].

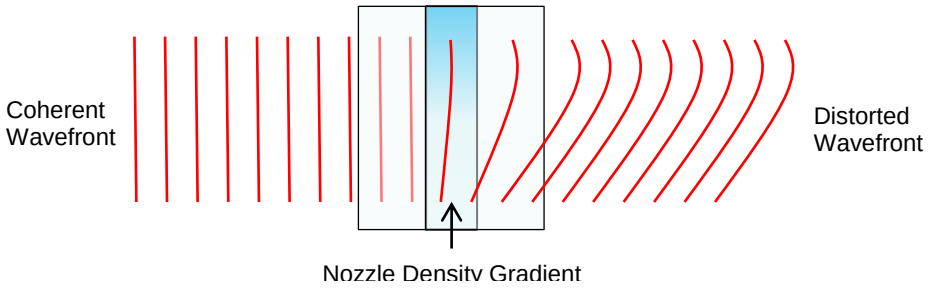

Figure 7: Wavefront distortion of a coherent beam as it travels through the density gradient of the nozzle

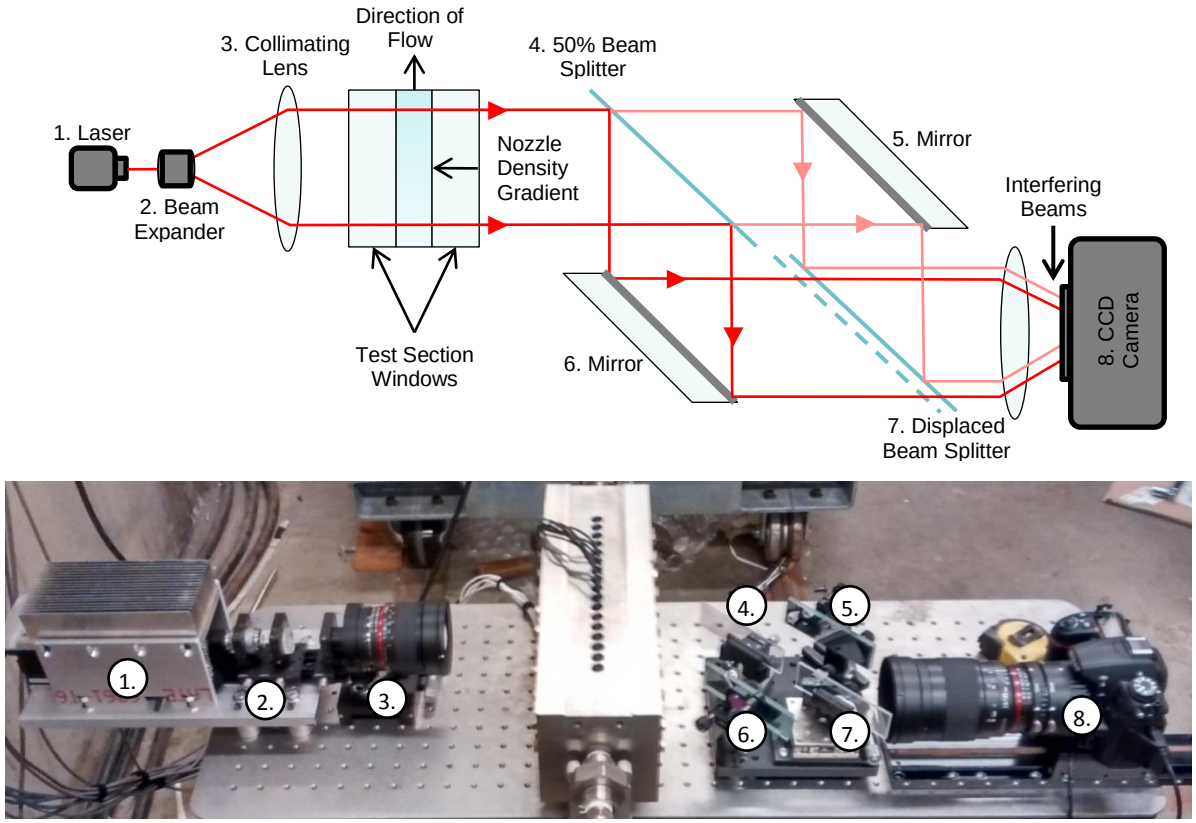

Figure 8: Schematic and image of the shearing interferometer used on the MIT CO_2 test rig

Interferometry is typically used for the aerodynamic analysis of ideal gases in external flows applications and the densities seen in the present experiment are two orders of magnitude larger than what is reported in the external flow literature [13]. This introduces new challenges in image analysis, since the interference fringes become narrowly spaced, requiring approximately 200 pixels per mm of view field. This necessitates a very high resolution CCD camera (~100 MP) to capture the raw images of the region of interest in the test section. The idea in the present paper is to measure density gradient instead of absolute density using a shearing interferometer so as to allow for a standard high-resolution CCD camera (16MP). Furthermore, a shearing interferometer is much more vibration tolerant and more robust with respect to optical defects than a conventional Mach-Zehnder Interferometer [13].

In a standard Mach-Zehnder interferometer, the phase-shifted beam that passes through the test section is compared with a coherent reference beam [11]. Because there are two separate beams the system is susceptible to vibration and precise control of the path length of the reference beam is necessary. A shearing interferometer, as used in this experiment, is a common path interferometer where a single beam is divided into two overlapping beams after passing through the test section. The beams are then combined with a spatial displacement, creating interference fringes. The fringe pattern is a measurement of the density change between the two paths and can be numerically integrated to calculate the absolute density of the gas.

The interferometer that was designed and built for the CO_2 test rig is shown below in Figure 8. A 50mW diode laser with a wavelength of 671nm and coherence length greater than 1m is expanded and collimated through a microscope objective and a standard camera lens respectively. The beam passes through the test section and experiences a phase lag as well as an angular deflection caused by density

changes within the gas. This deformation of the light is illustrated in Figure 7. Care has been taken to minimize refractive index bending by focusing on a plane at 1/3rd of the test section width from the beam entry point as described by [14]. After passing through the test section, the beam is split using a plate beam splitter. The beams are re-directed by two mirrors and then pass through a second beam splitter which recombines them into a single beam. By changing the position of the second beam splitter, the spatial shifting between the beams can be adjusted. The fringe pattern from these beams is then focused onto the CCD chip of a digital camera where the interference pattern is recorded.

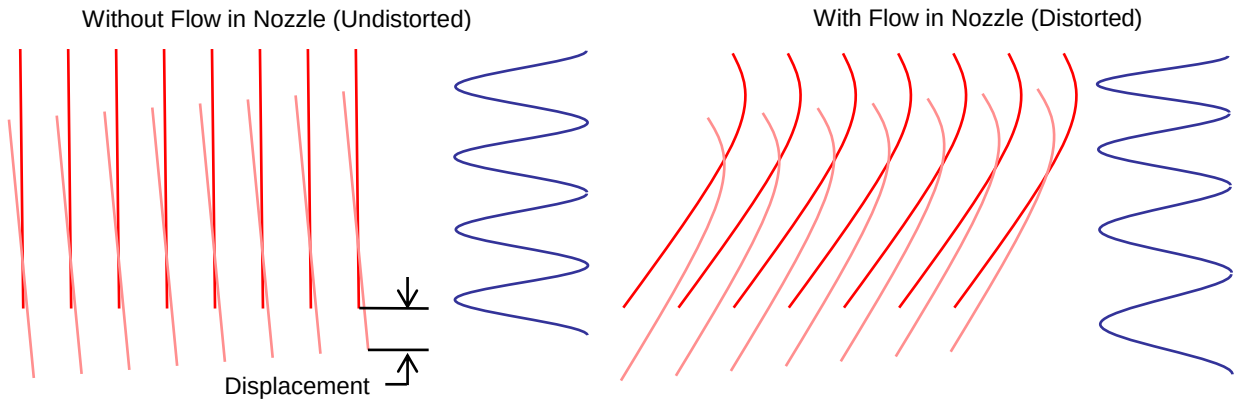

Figure 9: Effect of wavefront distortion on interference pattern. Note the stretched sinusoid in the case with flow.

A static fringe pattern (carrier fringes) is created by applying a rotation about the vertical axis to one of the mirrors. The amount of spatial displacement between the two beams compares the different optical paths through the flow as a phase shift, which adds or subtracts to the carrier fringe pattern. This spatial shift enables the shearing interferometer to measure quantitatively the density gradient within the flow. The rotated and shifted beams with and without distortion are illustrated in Figure 9.

The beam-splitter setup is a variation of a Twyman-Green interferometer, typically used for the quantitative evaluation of optical components. Moving the final stage beam-splitter, creates a linear displacement of the shearing images, whereas, applying a tilt to one of the mirrors produces a non-linear shift more associated with conventional qualitative shearing systems [15]. The combination of these approaches has several advantages.

1) It allows an accurate and linear displacement between the beams. This means that the interferometers measurement sensitivity can be adjusted over a wide range of operating conditions.
2) The path difference can be optimized, both to take account of the coherence of the light source and to accommodate the path length change due to density change experienced within the flow.
3) The amount of non-linearity and sensitivity of the system can be controlled accurately. This is an advantage at the numerical integration stage where the density gradient in the flow changes substantially from the start of the channel to the throat.

Precise knowledge of the displacement between the beams is key in extracting accurate quantitative data from the interference images, and a novel method was developed specifically for this rig.

Determination of Image Displacement

Displacements between the two legs of the beam-splitter are approximately 250 microns. An accuracy of 5 microns was required to achieve an uncertainty of approximately 2% for density measurements. Each pixel of the image is approximately 11 microns, which means that sub-pixel resolution accuracy is required. Initially measuring the displacement of a high-resolution ruler was used to determine the image offset. This gave an accuracy of approximately 30 microns, and was limited to directly measuring displacements greater than 250 microns due to the finite width of the lines being imaged. The large errors were mostly due to the inconsistencies of edge detection of the strips on the ruler.

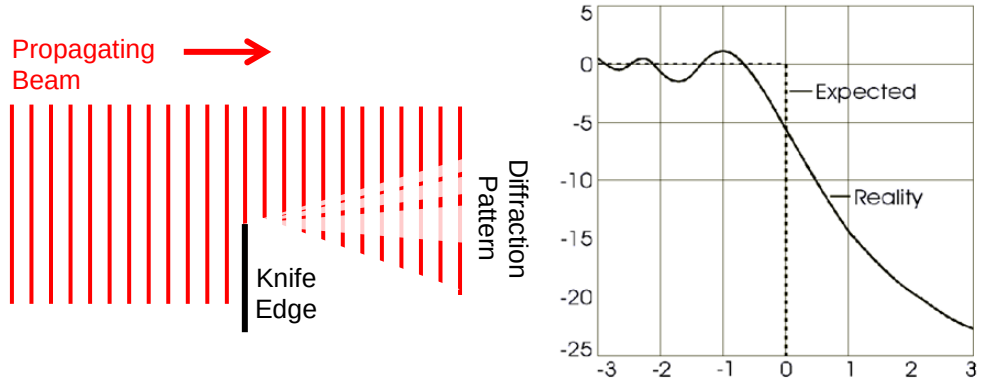

Figure 10: Qualitative illustration of a knife edge diffraction pattern and the comparison to a sharp edged discontinuity with the resulting oscillating diffraction pattern

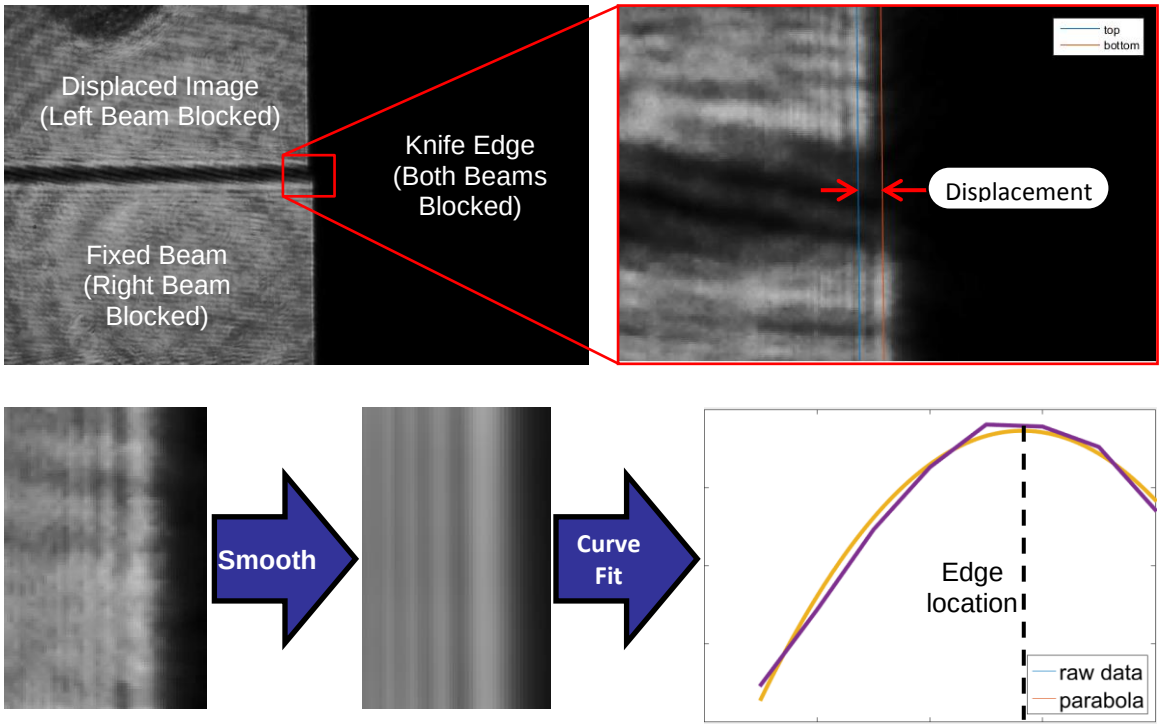

Figure 11: An example image taken with the knife edge and beam blocker and illustration of the image-processing that is required to track the edge and determine displacement

To alleviate the issues with edge detection, the ruler image was replaced with a knife edge, backlit by the laser described earlier. A knife edge lit in this manner creates a very distinct and repeatable interference pattern qualitatively illustrated in Figure 10. In order to measure the displacement of this knife edge in a single image, the beams travelling through the two halves of the beam splitter had to be segregated before entering the camera lens. This was achieved by a blocking plate which blocked the top half of one beam and the bottom half of the other beam. A schematic and image of the setup is shown in Figure 12 and 13 respectively

The interference patterns for the top and bottom beams are smoothed in the vertical direction using a moving average filter. A quadratic polynomial is fit to the points adjacent to the highest pixel value in each row of the image. This yields the theoretical location of the first maximum in the interference pattern to sub-pixel accuracy. A line is then fit to the point location s for the top and bottom edges and a displacement between the two is measured. This process is illustrated qualitatively in Figure 11. The

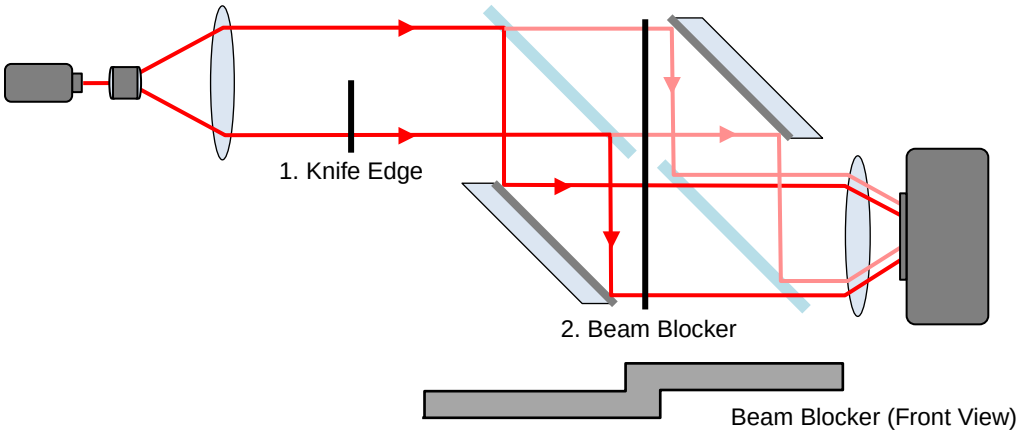

Figure 12: Top view of the interferometer setup with a knife edge in place of the test section and the beam blocker placed between the plate splitters

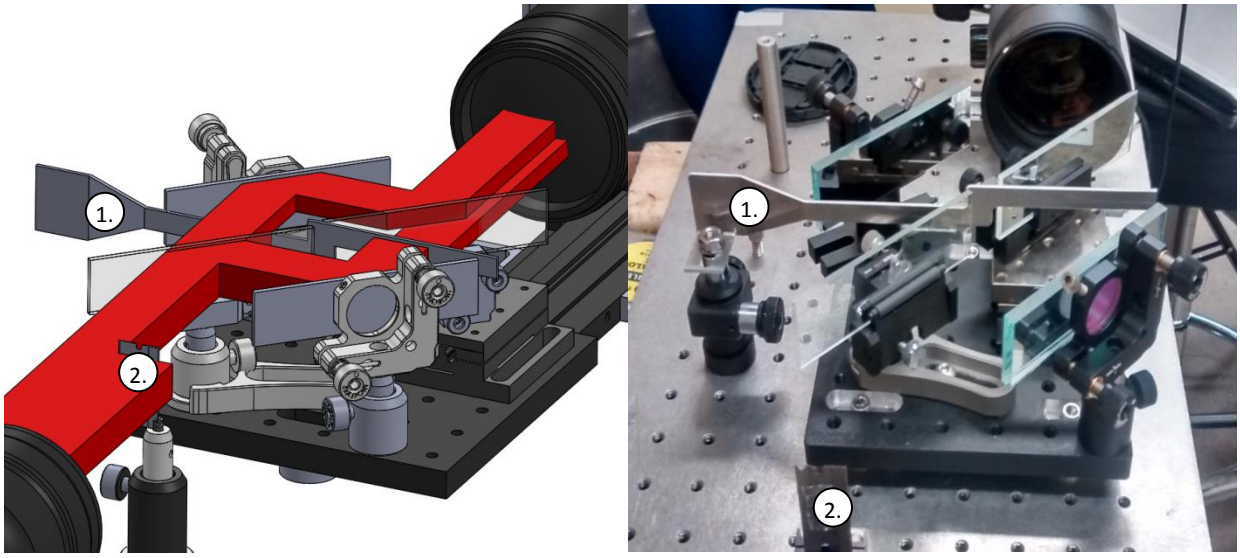

Figure 13: CAD model and image of the interferometer with beam-blocker in place. The red solid on the left illustrates the beam as it travels past the knife edge and through the beam-splitter. Note the displaced location of the top and bottom beams when they enter the lens

accuracy of this method is outlined in Table 1. Maximum Error was 4.36 microns and average error was 3.5 microns. This is approximately 1/3 of a single pixel width exceeding the initial goal of 5 micron accuracy.

Micrometer Setting [μm]	Calculated Displacement [μm]	Error [μm]
0	0	0
50	47.12	2.88
100	103.26	3.26
150	154.36	4.36

Table 1: accuracy of knife-edge based measurement method

Image Post Processing

Raw fringe images were post-processed using a Fourier transform based fringe analysis with the software Package UU [16].This analysis technique as well as other relevant methods of fringe image analysis are outlined in detail by Judge and Bryanston-Cross [17]. A qualitative illustration of this process for a 1-D sinusoid is shown in Figure 14

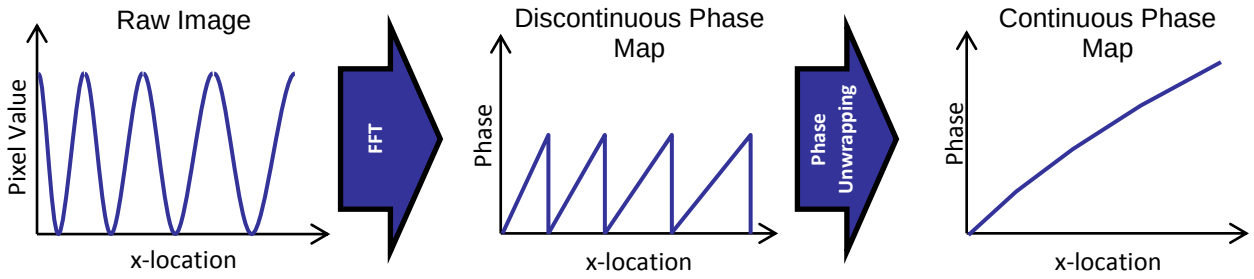

Figure 14: 1-D Illustration of the fringe filtering and unwrapping process

A progression of images through the various stages of post-processing is shown in Figure 15 for reference. The raw fringe image is first equalized along the length of the nozzle to bring the average brightness to a constant value (image 1). An FFT filtering process is applied, yielding a discontinuous phase map (image 2). Finally, a continuous phase map is produced by un-wrapping the discontinuous map. This is repeated for the conditions with and without flow in the nozzle. These are imported into 2-D data arrays and subtracted from one another yielding the derivative of optical phase difference due to the density gradient in the nozzle. By taking the difference between the flow and no-flow phase maps and dividing by the spatial shift between the two images, the derivative of phase lag can be calculated via

$$\frac{\partial(\Delta\phi)}{\partial x} = \frac{\Delta\phi_{flow} - \Delta\phi_{no\ flow}}{shift}$$

Numerical integration yields the phase lag due to the density gradient in the nozzle. Using the wavelength of the laser, the physical path length through the test-section and the known optical path length at the initial location, the phase lag can be converted to the optical path length difference and index of refraction by

$$\Delta l = \frac{\Delta \phi}{2\pi} \lambda_{laser} + \Delta l_0$$

$$n = 1 + \frac{\Delta l}{w_{test-section}}$$

Finally, the Lorentz-Lorenz equation [18] [19],

$$\rho_{[kg/m^3]} = \left(\frac{n^2 - 1}{n^2 + 2}\right)\left(\frac{3M}{4\pi\alpha N_A}\right)$$

is used to calculate density from refractive index where n is the refractive index, M is the molar mass, α is the molar refractivity, and N_A is Avogadro's number.

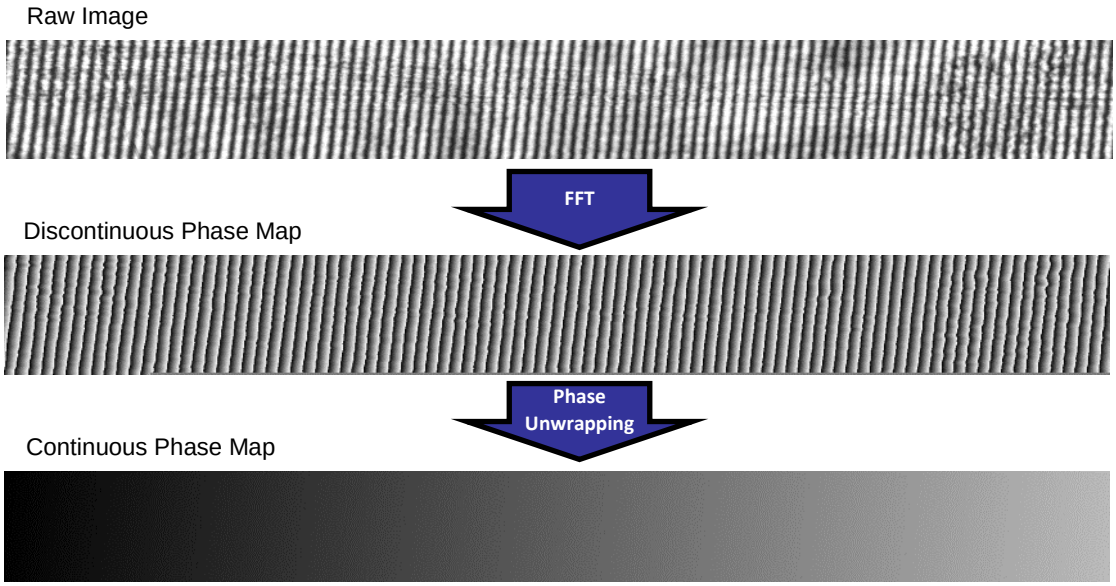

Figure 15: The steps of FFT image processing of interferometric images

Test Rig Measurement Results

While pressure measurements downstream of the throat were reliable and accurate when compared with the CFD calculations, density measurements were impossible due to Mach waves as seen in the inset of Figure 16. The Mach waves resulted from the unpolished surfaces of the nozzle inserts. Because of this, all comparisons made in this paper will be in the upstream section of the nozzle.

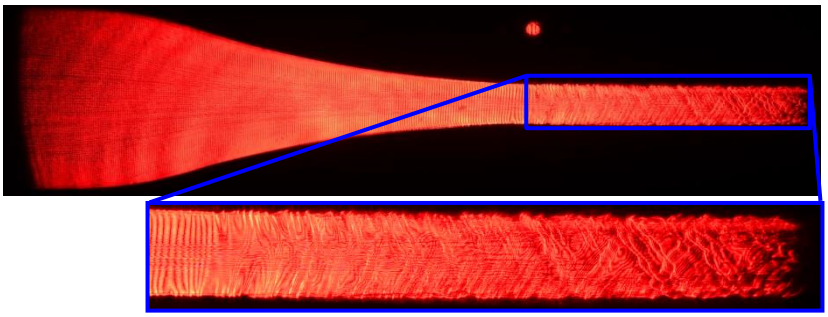

Figure 16: Image of the nozzle during operation showing distortion from Mach waves in the supersonic region downstream of the throat T_T = 325K, P_T = 22 bar

Verification of Experimental Test Rig

In order to ensure that the metastable properties can be accurately measured, the correct implementation of the experimental set up is verified through comparison with numerical calculations in the thermodynamic region at 10 bar and 320K where the flow behaves as an ideal gas and accurate measurement of the gas properties are available through the NIST database. The experimental pressure measurements agree well with the CFD results, showing a maximum deviation of 3%. The maximum sensor error at these pressures is 1%

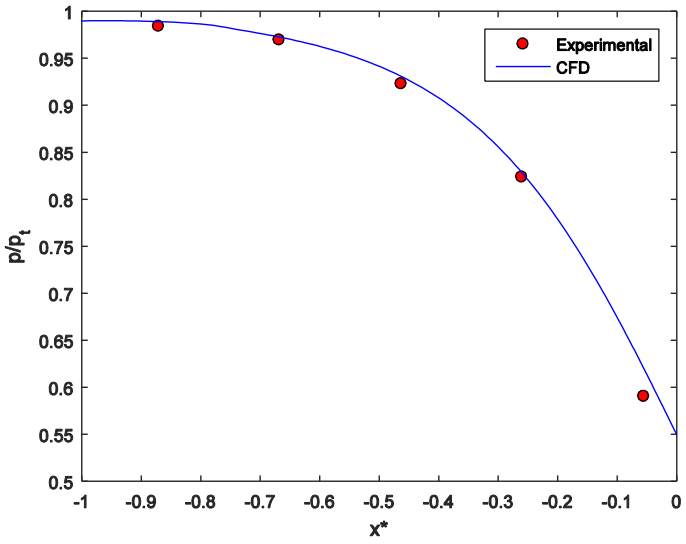

Figure 17: Comparison between experimental pressure measurements and those calculated with CFD showing good agreement T_T = 320K, P_T = 11bar

Operating Conditions

Typical stage inlet total temperatures for a multi-stage centrifugal S-CO2 compressor are approximately 315-330K, approximately 10-25 degrees above the critical temperature. The maximum Mach numbers in the vicinity of the leading edge are low supersonic (<1.2) [6]. Due to the aforementioned challenges in measuring the density past sonic conditions due to Mach waves in the diverging section, the total

temperature and pressure of the tank were brought close to the saturation dome. For each run, minimum total temperatures were limited by a 5K delta over either ambient (295K) or the saturation temperature, whichever was higher. This allowed for the rig to reach static temperatures similar to those observed in a typical supersonic impeller blade. Figure 18 illustrates the range of thermodynamic states in terms of temperature and entropy that can be reached using the sonic expansion only. The shading values at all points represent the Mach number in a typical compressor with an inlet total temperature of 315K. The maximum compressor Mach numbers are 1.1-1.2 for all runs, demonstrating that the entire temperature range of interest can be explored with only a sonic expansion. Additionally, Figure 18 illustrates the large range of metastable conditions that can be achieved in the nozzle.

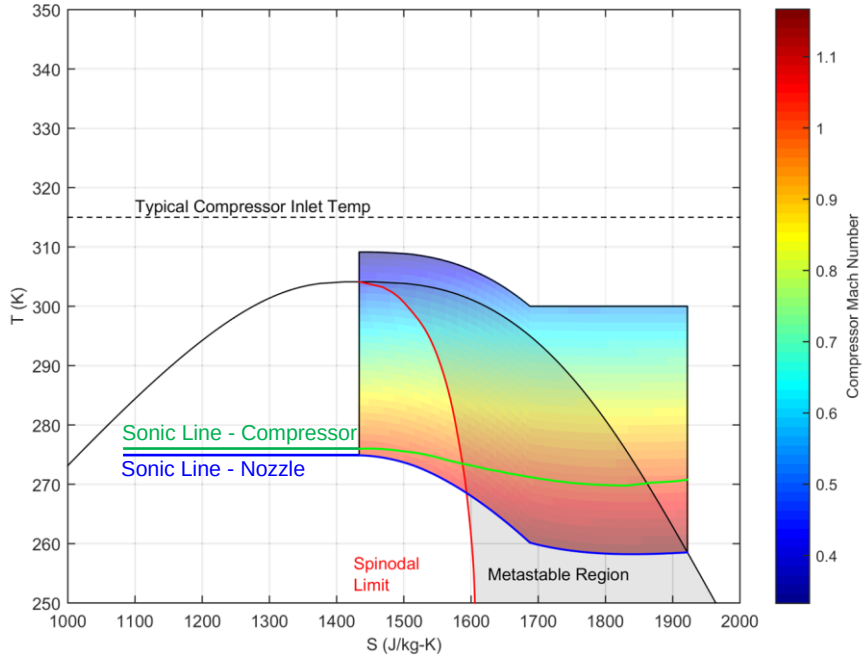

Figure 18: T-S Diagram of the operating range showing compressor Mach numbers and the sonic line of the experimental nozzle. Also shown are the spinodal limit and the approximate metastable region

Validation of Metastable Properties Extrapolation

To validate the shearing interferometer, density measurements were compared with those calculated from the pressure measurements. The total temperature is known from the stagnation conditions in the tank, and the total pressure can be determined based on the area ratio and the pressure measurement at the first pressure transducer location. Due to the high Reynolds number of the flow (of order ~10^7), viscous losses are small, and the entropy calculated from the stagnation conditions can be assumed constant throughout the nozzle. Pressure and entropy fully define the state of the fluid, and NIST RefProp was used to calculate the corresponding densities at all the pressure transducer locations.

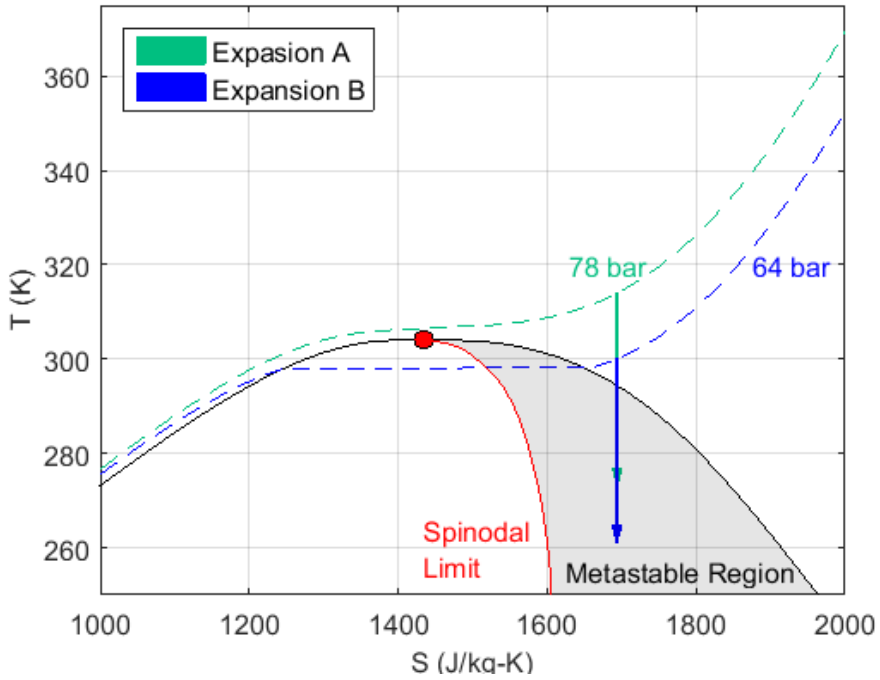

Figure 19: T-s Diagram illustrating the two blowdowns used for comparing the metastable extrapolation methods

Figure 20 and Figure 21 compare the measured and calculated densities for blowdown runs with total conditions at 315K and 77bar, and 301K and 67 bar respectively. The total conditions for expansion A were chosen based on typical stage inlet temperatures for a supercritical CO_2 compressor. This led to a relatively small excursion into the metastable region. To push the limits of condensation and maximize the excursion into the metastable region, expansion B was performed at the same entropy as that of expansion A, but with a reduced total temperature of 301K. These conditions are illustrated on a T-S diagram in Figure 19.

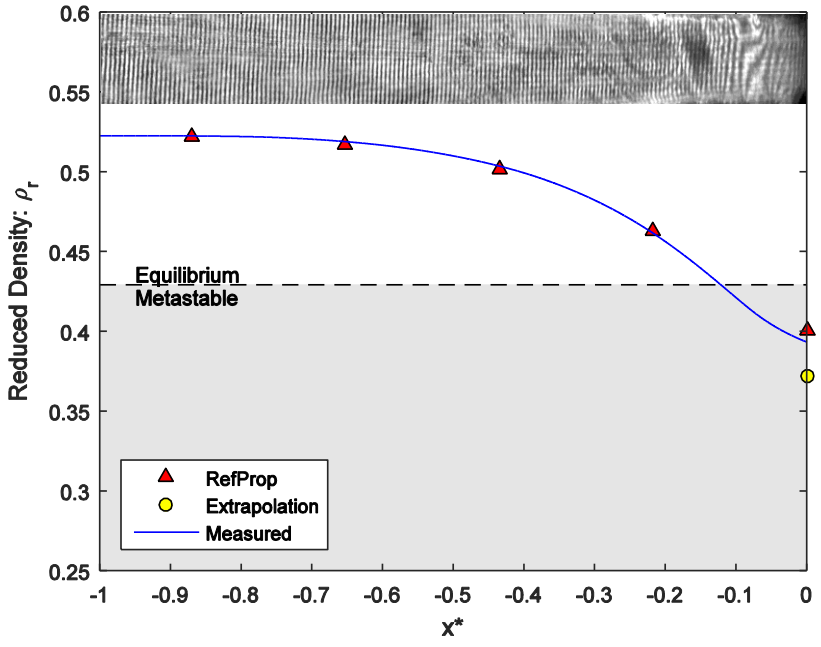

Figure 20: Density comparison for supercritical blowdown showing good agreement for both equilibrium and EOS and extrapolation based metastable conditions. T_T = 315, P_T = 77 bar

In Figure 20 and Figure 21, the points above the indicated saturation line are at equilibrium conditions, and can therefore be computed using the above method and the Span-Wagner EOS directly. The density measurements agree well for the equilibrium measurement points showing a maximum error of less than 0.5%. The comparison between wall pressure measurements and centerline density measurements at the same axial location assumes that streamline curvature effects are negligible, and this is not the case throughout the nozzle. This explains some of the discrepancy between the measured and calculated densities.

The comparison points in the gray region below the saturation line use metastable properties calculated from the tabular and EOS based extrapolation methods discussed in the Technical Approach section. For expansion A, the measured density agrees well with the extrapolated value, confirming that interferometry can be successfully used to measure metastable properties in a high-speed, high density flow. Errors below 5% between measured and calculated property values by direct extrapolation indicate that this is a viable strategy for supercritical conditions away from the critical point. EOS based extrapolation gives better agreement, with errors less than 2%, giving a preliminary indication that this is a more appropriate method for calculating metastable properties. The fact that it is already implemented in commercially available software (RefProp) also makes it a more attractive option than the tabular extrapolation method.

Expansion B demonstrates the ability of the rig to identify condensation onset. Scattering and blockage of the beam by droplets in the nozzle prevented any density measurement past the condensation front at approximately the location of the 4th pressure transducer. This can be seen by the black region in the fringe image overlaid with the plot shown in Figure 21. A fringe image without condensation occurred in expansion A and is illustrated in Figure 20.

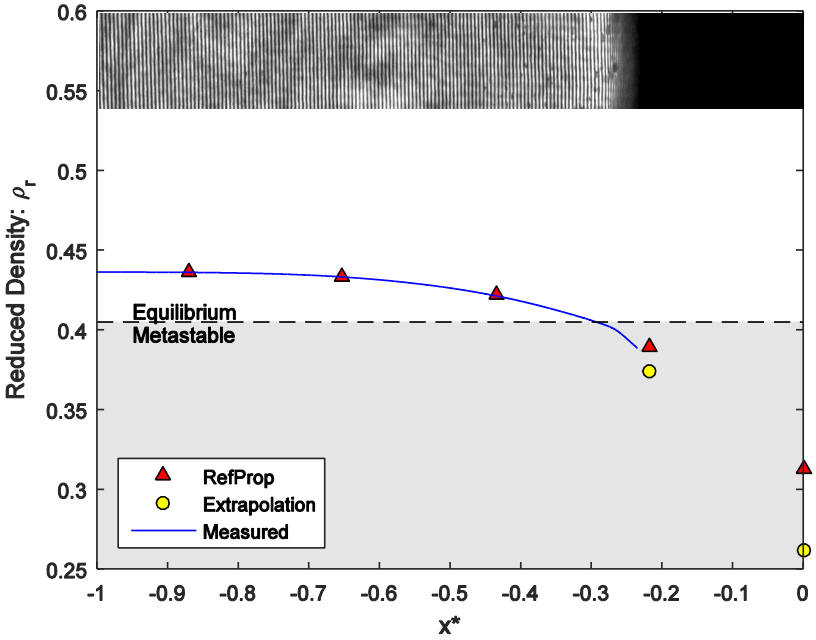

Figure 21: Density comparison for T_t = 301K, p_t = 67 bar. Note the onset of condensation near the 4th pressure transducer illustrated In the overlaid fringe image

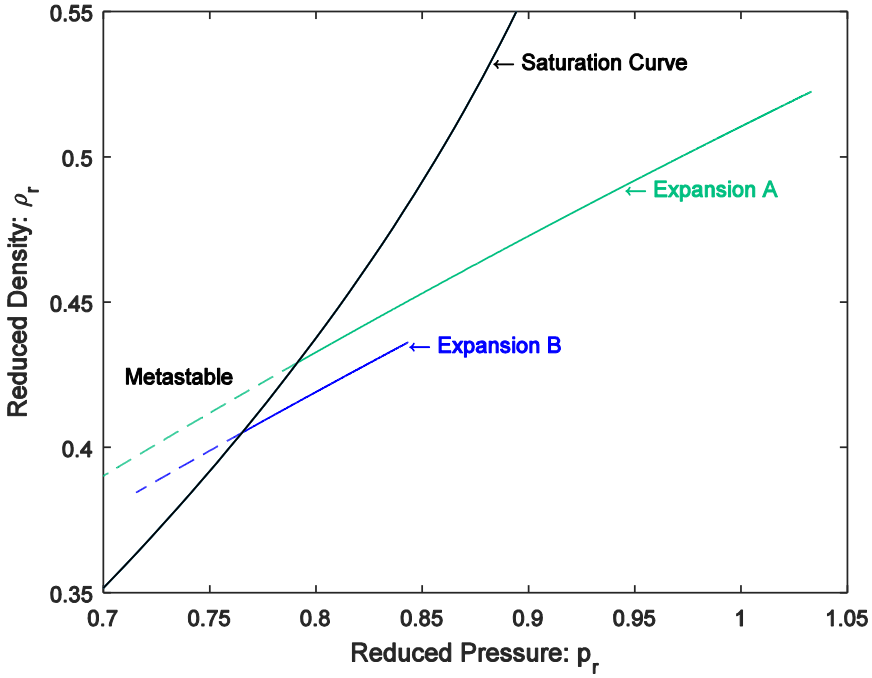

Figure 22: expansion A and B plotted on axis of reduced density and reduced pressure. Metastable conditions are shown as dotted lines

Similar to Figure 3 reduced density vs reduced pressure are plotted in Figure 22 with the conditions for the two expansions A and B characterizing the metastable state. Despite similar vicinity to the critical point, expansion A demonstrated a larger excursion into the metastable region. Work is ongoing to determine the cause of this difference, but it is currently thought to be related to varying residence times in the nozzle and the vicinity of the total conditions to the vapor dome.

Conclusion

This paper demonstrates the first measurements of supercritical metastable CO_2 using a first-of-its-kind high density shearing interferometer. Additionally, the results confirm the viability of interferometry and pressure measurement as a means of fully characterizing the thermodynamic state of metastable CO_2, and verify the validity of two approaches using direct extrapolation of metastable properties.

It is still unknown under what range of conditions the measurement and extrapolation scheme will hold. To further verify the feasibility of the proposed extrapolation methods and to identify their limits additional experiments are required. This will be pursued in future work by: (1) Conducting systematic analysis at different operating conditions approaching the critical point to allow for larger gradients in the flow properties, and (2) extending the interferometric measurement method to the supersonic section of the nozzle to assess the impact of different expansion rates [2].

Acknowledgment

This research was funded by Mitsubishi Heavy Industries Takasago R&D Center, which is gratefully acknowledged. In particular, the authors would like to thank Dr. Eisaku Ito, and Mr.Akihiro Nakaniwa for their support.

Sources

[1] Rinaldi, E., Pecnik, R., and Colonna, P., 2013, "Steady State CFD Investigation of a Radial Compressor Operating With Supercritical CO2," ASME Paper No.GT2013-94580.

[2] Lettieri C, Yang D, and Spakovszky Z. "An Investigation of Condensation Effects in Supercritical Carbon Dioxide Compressors". ASME. J. Eng. Gas Turbines Power. 2015; 137(8):082602-082602-8. doi:10.1115/1.4029577.

[3] Ryzhov, Y.A., Gorbunov, V. N., and Pirumov, U. G.. "Nonequilibrium condensation in high-speed gas flows". New York: Gordon and Breach Science Publishers, 1989. Print.

[4] Duff, K.M., 1964, "Non-Equilibrium Condensation of Carbon Dioxide in Supersonic Nozzles," M.S. thesis, Dept. of Mech. Eng., Mass. Inst. of Tech., Cambridge, MA.

[5] Guha A. "Thermal Choking Due to Nonequilibrium Condensation". ASME. J. Fluids Eng. 1994; 116(3):599-604. doi:10.1115/1.2910319.

[6] Baltadjiev ND, Lettieri C, Spakovszky ZS. "An Investigation of Real Gas Effects in Supercritical CO2 Centrifugal Compressors". ASME. J. Turbomach. 2015; 137(9):091003-091003-13. doi:10.1115/1.4029616.

[7] International Association, 2007. "International Association for the Properties of Water and Steam: Revised Release on the IAPWS Industrial Formulation 1997 for the Thermodynamic Properties of Water and Steam". IAPWS Release, Switzerland, 2007.

[8] Span, R. and Wagner, W., "A New Equation of State for Carbon Dioxide Covering the Fluid Region from the Triple-Point Temperature to 1100 K at Pressures up to 800 MPa"

[9] Lemmon, E.W., Huber, M.L., McLinden, M.O. NIST Standard Reference Database 23: Reference Fluid Thermodynamic and Transport Properties-REFPROP, Version 9.1, National Institute of Standards and Technology, Standard Reference Data Program, Gaithersburg, 2013

[10] Lamanna G., van Poppel, J., and van Dongen M.E.H.. "Experimental Determination of Droplet Size and Density Field in Condensing Flows," Experiments in Fluids, 32(3), p.381, 2002

[11] Settles, G.S. "Schlieren and shadowgraph techniques : visualizing phenomena in transparent media". Berlin New York: Springer, 2001. Print.

[12] Timmerman, B.H., Bryanston-Cross, P.J., Skeen, A.J., Tucker, P.G., Jefferson-Loveday, R.J., Paduano, J, Guenette, Jr., G. R.. "High-Speed Digital Shadowgraphy for High-Frequency Shock Tracking in Supersonic Flows". The 17th Symposium on Measuring Techniques in Transonic and Supersonic Flow in Cascades and Turbomachines Stockholm, Sweden (2004)

[13] Mercer, C.R., and Raman, G. "Quantitative Interferometry in the Severe Acoustic Environment of Resonant Supersonic Jets", AIAA Journal, Vol. 40, No. 3 (2002), pp. 438-442

[14] Merzkirch, W. *Flow Visualization: Second Edition*. Orlando FL; Academic Press, 1987

[15] Pelliccia-Kraft, B. J, Watt, D. W.. "Three-dimensional imaging of a turbulent jet using shearing interferometry and optical tomography". Exp. in Fluids, Vol. 29, Issue 6, pp 573-581, Dec. 2000

[16] Lujie, C. "Cross-platform Image-processing Program – UU", Singapore Inst. of Tech. & Design. 2014

[17] Judge, T.R, and Bryanston-Cross, P.J., "A Review of Phase Unwrapping Techniques in Fringe Analysis," Optics and Lasers in Engineering, Vol. 21, Issue 3 (1994) pp. 199-239

[18] Lorentz, H.A. "On the Relation Between the Propogation of Light and Density of a body", Ann. Phys. vol 9, pp. 641-665 (1880)

[19] Lorenz. L., "About the Constant of Refraction", Ann. Phys. col 11, pp. 70-103 (1880)